Bachelor Graduation Project

Radar Based Human Vital Signs Detection in Cars

State of the Art Analysis

Delft University of Technology

Jasper Massey

4478215

Emiel van Veldhuijzen

4480198

July 14, 2020

TU Delft Delft University of Technology

Faculty of Electrical Engineering, Mathematics and Computer Science
Delft University of Technology

State of the Art Analysis

Authors:
Jasper Massey

Emiel van Veldhuijzen

Supervisor:
Francesco Fioranelli (TU Delft)

Foreword

This report was written after two months of diving into the world of technologies that are capable of detecting human beings. Many technologies were found and investigated, and the best technologies are discussed in this report. The motivation behind the investigation is to prevent babies from being left behind in cars and dying due to an heatstroke. In the end, a recommendation is given for the best suitable technology for this implementation. We want to express our gratitude to our supervisor Francesco Fioranelli, who did great in bringing over knowledge and suggestions when needed and was always available to help us out. And also for making the project and the communication possible and easy in times of COVID-19. Also, Ioan Lager receives our gratitude for organizing the bachelor graduation process in times of COVID-19, providing clear and relevant information for guidance.

Contents

1 Introduction

In this chapter the goal of the project will be defined. The approach of the project will be explained and the goal of this thesis will be specified. Also, an overview of the thesis will be given.

1.1 The goal of the project

In the world, numerous babies die from heatstroke as a result of being left behind in a car. In the United States alone, on average 36 children die each year because of this [1], this should be prevented. Using today's technologies it is possible to detect humans in various ways, these technologies are already widely used in security systems and medical surveillance. Our project group will implement a non-contact detection system in the car, based on radar technology, in order to prevent the situation where a baby is left behind in a car. Since a hardware prototype is not possible due to the current circumstances, the detection system is approached from a more theoretical point of view.

1.2 Division

The project is divided into smaller groups where each group tackles different problems of the implementation of the radar system. The three subgroup where the project is divided in are:

- State of Art Analysis Group
- System Analysis Group
- Signal Processing Group

The goal of our subgroup, state of art analysis, is to compare the suitability of using radar for our implementation and provide evidence for or against its performance in comparison to other detection technologies suitable for this application, e.g., sonar and infrared. The hardware implementation of the radar system in the car will be done by the system analysis group. The signal processing group focuses on the signal processing algorithms, as well as the hardware implementation of the processes that occur in the algorithm. The theses of the hardware group and signal processing group can be found in [2] and [3] respectively.

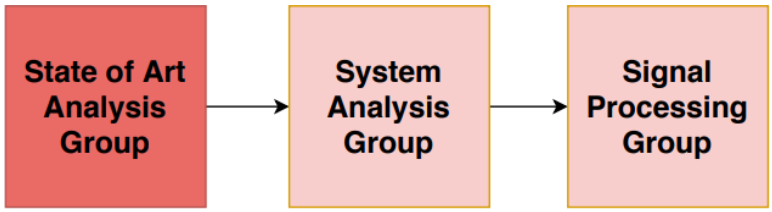

Figure 1: Overview of the project subgroups

1.3 State of Art Analysis

The goal of the whole project is to detect the presence of a baby in a car. We will implement a system based on radar, however, there are many different technologies that are used for the detection of humans.

In this thesis, the State of Art Analysis, the use of radar for our implementation will be substantiated, with respect to other technologies that would seem suitable. Detecting the presence of a baby in the car is achieved through the detection of the respiration or heartbeat. Detection of such signals does not necessarily imply the estimation of their rate (i.e. how many respiration or heartbeat cycles are performed), but in first instance as the capability to just distinguish the presence of such signals from the background of the empty car. The estimation of the rate can be thought of as a further, more advanced capability. Detecting the respiration is expected to be easier than heartbeat because the involving movement of the chest due to respiration is larger than with heartbeat.

To get a good impression on the variety of technologies capable of detecting humans, several technologies will be mentioned and explained briefly. These technologies are categorized by *contact-based* and *non-contact* based techniques. After that, a selection is made where we drop the technologies that are not worth further investigation, because they do not satisfy the basic criteria for our purpose.
For the chosen promising technologies, an in-depth investigation on existing systems that use the specific technology will be done. In addition for radar, the difference between using different signal properties is discussed, before an in-depth investigation is done for our radar system. The in-depth investigation will be a technical assessment done from an electrical engineering background. The research will consist of a list of technical aspects that will be discussed per technology.
Finally, based on these technical aspects, a good comparison between the promising technologies is done, and evidence for and/or against the use of our radar will be given.

1.4 System Engineering Approach

To perform a respectable State of Art analysis, our approach is informed by a formal System Engineering approach, described in the Masters Course EE4C02, based on the book *Introduction to Systems Engineering* [4]. This implies that first the problem will be clearly defined. A programme of requirements is then set to achieve a solution to the problem. These requirements are decomposed into mandatory and trade-off requirements. The mandatory requirements will indicate whether a system is suitable at all or not. Trade-off requirements will be investigated for the suitable systems, to be able to make a comparison based on those requirements. These trade-off requirements correspond to the earlier mention technical aspects in Section 1.3

1.5 Structure

The structure of this thesis is as follows. In Chapter 2, the program of requirements will be listed and explained. In Chapter 3, many various technologies will be discussed and criticized. The most promising technologies, infrared, optical cameras and sonar, will then be elaborated and investigated in-depth in Chapters 5 and 6. For the radar technology, the differences between various radar systems are discussed in Chapter 4 and an in-depth investigation will be done for the most suitable radar system. In Chapter 7, all pros and cons of the investigated systems will be listed in a table for comparison. Evidence for and against the use of radar will be discussed using this table. Finally, in Chapter 8, a conclusion is made and some suggestions to continue the work are given.

2 Programme of Requirements

2.1 Problem Definition

In our study, options for the detection of people inside cars are investigated and discussed, in particular to avoid the situations where babies are forgotten in locked vehicles for a long time. Important vital signs for the detection of living beings are body temperature, heart rate, respiration rate, blood pressure, etc. To examine the presence of a baby, the goal of our system is to detect at least one of them, specifically respiration rate, to conclude that there is a living being in the car when this specific vital sign is detected. The steps that the analysis will consist of are:

1. Breathing detection
2. Heartbeat detection
3. Respiration rate and heartbeat estimation

Respiration will have the primary focus, because it is easier to detect with most of the technologies. The next step is to detect heartbeat, because for most technologies this would be based on the same principle, but based on smaller movements. When it is proven that respiration rate and heartbeat are detectable, the possibility for an accurate estimation for both of these vital signs is investigated.

The system that will be implemented to accomplish this respiration rate and heartbeat detection will be based on radar. However, besides radar, various other technologies are capable of detecting respiration rate and heartbeat nowadays. Research on these other technologies will be done to reach the goal of our project: Provide evidence for or against the use of radar, in comparison with other human detection technologies. To be able to compare, some requirements are set in Section 2.2 to quantify the success of a technology.

2.1.1 System Implementation Overview

For the implementation in a car, it is assumed that for all technologies the system sensor will be implemented in front of the baby at a distance of 0.5 to 1 meter. Babies and toddlers are obligated to be seated in a child seat until they reach the age of 4. It is assumed that the child seat will be placed on the backseat, since that is the most safe for the baby. When the child seat is placed forward, the location of where the system will be placed is illustrated in Figure 2. The child seat can also be placed backwards, in that case the system would be shifted to the right, the location indicated in the Figure by the star. The region of interest would in that case be reversed.

Figure 2: Illustration of the proposed location of the implemented system [5]

2.2 Requirements

To compare different technologies, some requirements are set. A distinction is made between mandatory and trade-off requirements. The mandatory requirements are discrete requirements and must be satisfied at all times. The trade-off requirements are desired criteria that are used for comparing the technologies.

2.2.1 Mandatory requirements

The mandatory requirements will support the first broad investigation into all possible human detection technologies. These requirements will measure whether a technology is worth implementing in a car for our problem or not. These requirements consist of:

The system

- must be able to detect the respiration or heartbeat of a person in a car
- shall not have any form of direct contact with the human, to avoid loss of comfort and to avoid remembering to actually connect some sensor to the baby
- must operate autonomously, without a person controlling it, to make sure that it can not be forgotten to start the system
- should be smaller than 5 dm^3 to make sure it can be implemented in a car without obstructing anything or anyone without changing the car layout
- must operate independent of the car's power state (on/off)
- must have an operation time of at least 2 hours to have a big enough time window to reliably and accurately detect the baby

- must be able to operate in a temperature range of 0°C to 70°C, where 70°C is the measured air temperature in a car after 4 hours in the sun with an outside temperature of 40°C
- must be compliant with either the EMC Product Standards and the Automotive Industry Standards

2.2.2 Trade-off requirements

The technologies that are worth further investigation, i.e., those that comply with the mandatory requirements, will be represented by an existing system based on that technology. The trade-off requirements are used to quantify the success of that particular technology implementation. The trade-off requirements are to:

- minimize the power consumption of the system
- minimize the physical size of the system
- minimize the influence of ambient light on the detect-ability of vital signs
- minimize the influence of the temperature in the car on the detect-ability of vital signs
- minimize the cost of the system
- minimize the data complexity of the system
- maximize the heartbeat rate estimation accuracy of the system
- maximize the respiration rate estimation accuracy of the system

Based on these trade-off requirements, an investigation into system implementations will enable a good comparison between several suitable technologies.

3 Human detection technologies

In this chapter, many different technologies will be discussed and criticized. The overview of how the technologies are classified is shown in Figure 3. The first very broad look will consist of a distinction between *contact* and *non-contact* ways of detecting a person. Of course, the contact-based technologies are out of our scope, but their basics give a good impression on how the detection of a person can be done. Diving deeper into the non-contact based technologies, a distinction can be made between technologies using *electromagnetic* (EM) waves and *sound* waves. Subsequently, the techniques using EM waves are then divided into radar and several optical technologies. This division is chosen as it puts radar in a center point, connected with slight differences to all other technologies, which is favourable for the comparison.

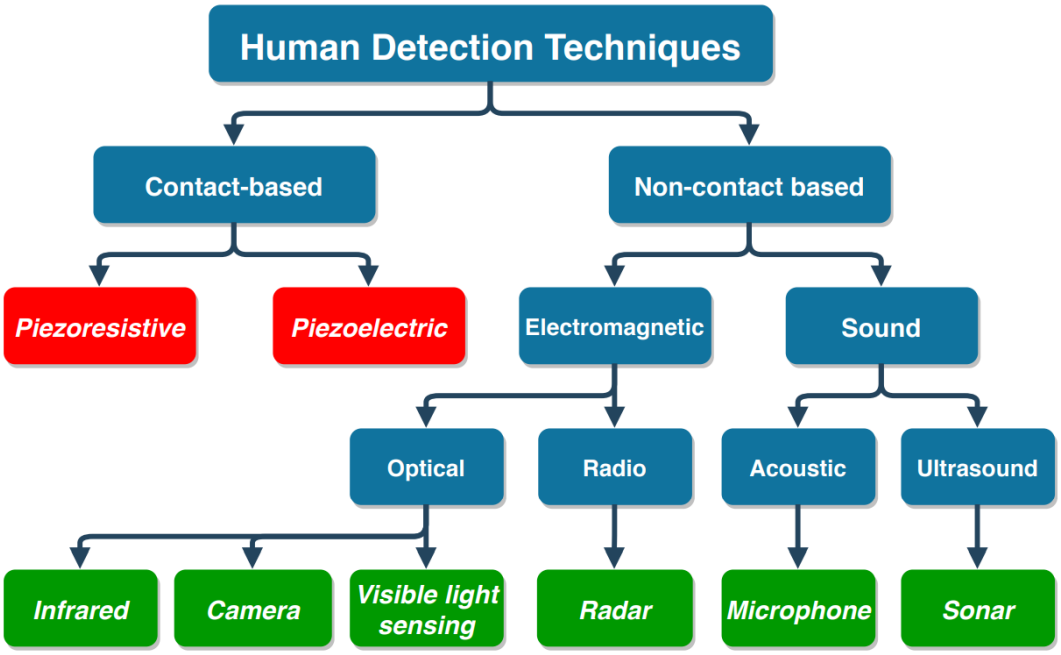

Figure 3: Overview and the classification of human detection technologies

In Table 1, the similarities and differences for these 6 technologies are listed. Given that radar is an active system using waves in the EM spectrum, this shows why these technologies are chosen to be able to make a good comparison.

	Passive/Active	**Spectrum**
Radar	Active	EM (Radio)
Visible light sensing	Active	EM (Optical)
Infrared	Passive	EM (Optical)
Optical Camera	Passive	EM (Optical)
Sonar	Active	Sound (Ultrasound/Acoustic)
Microphone	Passive	Sound (Acoustic)

Table 1: Similarities and differences of the 6 non-contact technologies

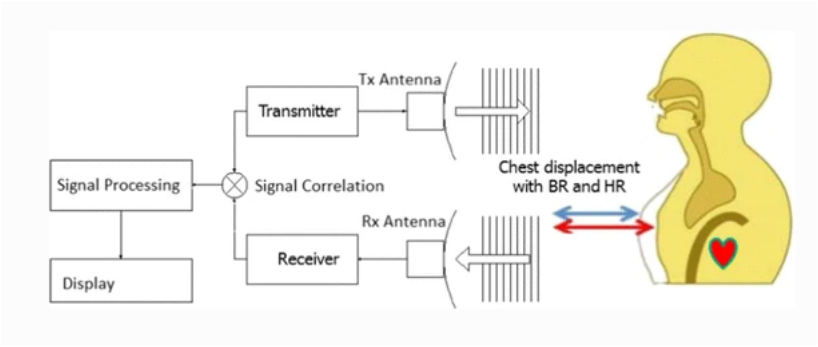

Figure 4: Basic overview of radar in the context of chest measurement[7]

3.1 Non-contact based technologies

3.1.1 Radar

A basic overview of how a radar (RAdio Detection And Ranging) system is used in vital sign detection is illustrated in Figure 4. Here separate antennas are used for transmitting and receiving. However, it is also possible to have one single antenna which both transmits and receives. Radio waves are electromagnetic waves in the frequency range of 30 KHz-300 GHz. However due to the mandatory dimension restriction, the antenna size is restricted. This results in a carrier frequency that is 1 GHz or larger. In the setting of the baby in a car, radio waves can be transmitted and echo back from the baby to the receiver. The observed echo can have changes in its amplitude, frequency and phase. Research in the past already use radar systems to detect vital sign. For example, a radar system exploited the Doppler effect [6].
A radar based on the Doppler effect exploits the fact that the received signal will return with a frequency depending on the change of distance with respect to time between the object and the radar. This allows to obtain information about breathing based on the frequency of the echo. More information about the Doppler effect in the received signal is given in section 4.2.1. Using radar to detect human vital signs has several advantages. The main advantages are that it is wireless, low cost, power effective, weather independent and accurate [6].

3.1.2 Infrared

The common technology that is used to detect humans within the infrared range of the electromagnetic spectrum is thermal imaging (infrared thermography, IRT). IRT is a non-invasive, non-contact technique which allows one to measure and visualize infrared radiation [8]. Using Stefan–Boltzmann law, we can see that an object, a human in our case, emits thermal radiation. The energy of this infrared radiation that is emitted increases when the temperature of that object increases [9]. With automated image processing algorithms, an image can be created using this radiation, as shown in Figure 5 [10] [11]. With suitable infrared signal processing technologies, the presence of a human can be determined [12].

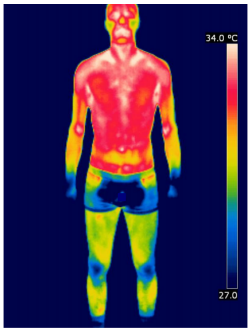

Figure 5: Infrared thermal images of the anterior body

Thermal imaging is used in today's thermal cameras. These cameras can be a suitable option to detect humans in a car. The fact that the technique is non-invasive, non-contact and anonymous, makes it very attractive for our purpose. Another asset is that it doesn't depend on visible light and can be used when there is lack of vision due to, for instance, smoke. Furthermore, if we want to acquire extra information about the detect human, it is possible to measure both breathing rate and exhaled air temperature, when using a sufficient precision [13]. However, a major downside when applying thermal imaging is that the resolution of the images will be very dependent on car temperature. The temperature of a parked vehicle was found to range from 20-30°C higher with respect to the outside temperature [14]. When the car temperature approaches the body temperature of roughly 37°C, it will become difficult to extract a human body from the thermal image and the system will always have a blind spot [15]. Therefore, to achieve a system that complies to our requirements, it is possible to solely depend on thermal imaging, but would be challenging when the car temperature matches the body temperature range.

3.1.3 Camera

Optical technologies on the basis of visible light, are commonly used for human detection, for instance in gait analysis laboratories [16] and security systems [17]. It is usually implemented by digital images and digital video systems, which are, respectively, pictures and movies that have been converted into a computer-readable binary format consisting of logical Os and 1s. Image processing is used to create the images and videos [18], where the available information can then be extracted and used to analyze properties of dynamic physical phenomena, such as the human body. The detection of vital signs (respiration and heartbeat) is done using images of the facial area, illustrated in Figure 6.

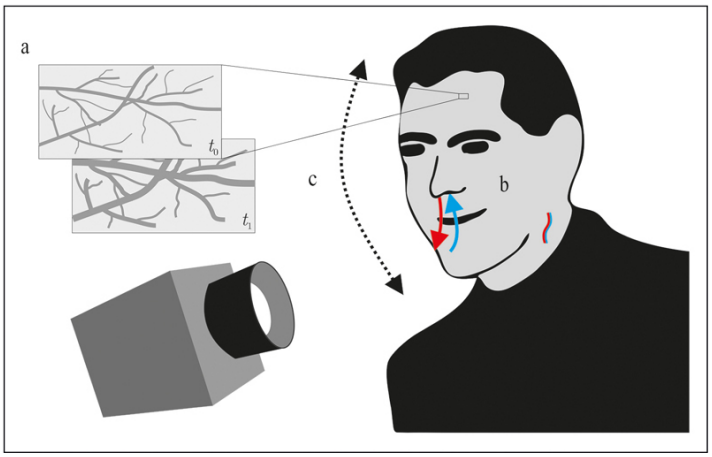

Figure 6: Illustration of three principles used for camera-based human detection [19]: a) slight variations of the optical properties of the human blood vessels b) systems using a built-in infrared camera to exploit temperature changes due to respiration and blood flow, and c) motion-based methods detect slight motion of the head (or other parts of the body) related to cardiac or respiratory activity, for instance used for defining the region of interest.

Optical methods using visible light requires complex calibration and prior knowledge about the human subject [20]. The images require signal processing for heavy data streams, and

computational resources for enhanced resolution [21]. However, many systems are already able to achieve that, and keep improving. Optical systems are however dependent on conditions like ambient light and smoke. Another point of attention is that optical technologies can create high resolution images of people, which could obey privacy regulations when not handled correctly [22]. Since optical cameras are really improving in heartbeat and respiration detection, a system in our car based on optical cameras would seem suitable.

3.1.4 Visible light sensing

Another technique in the optical visible light range is visible light sensing (VLS). Where for instance RF-based methods use RF signals and physical movement of the body, a visual-based method uses ambient light and the skin absorption. VLS is safe and is present everywhere during the day and is gaining significant interest, including human detection system [23]. However, when VLS is applied to detect humans and vital signs in cars, the constantly changing light would be a challenge, especially in dark circumstances. The detection of vital signs such as heartbeat and respiration is possible using VLS, but require very accurate data. With the changing lighting in a car, and in darkness, that would be very challenging.

3.1.5 Sonar

Sonar systems are another possibility for the detection of humans. Sonar systems can give a precise localization of an object and contain spectral information in a large bandwidth that can be used to detect object structure and sometimes composition [24]. A sonar system consists of an ultrasonic transmitter and receiver. It transmits a pulse to the medium of interest, and from its echoes, it can construct an image of the objects and activities in the medium, as shown in Figure 7. When a human sits in a car, the presence and motion of various components of the body including the head, torso, arms, legs, and feet produce an acoustic signature. Applying automatic recognition on the acoustic signature can then provide us information the presence of humans [25].

The advantages of this technology with respect to our requirements are that it does not require attaching markers to different body parts, it can work under any light condition, and in the presence of smoke during a fire, or high humidity conditions, and it maintains the privacy of the subject. Sonar systems mostly track large motions of the human body [26], but it is possible to obtain information about respiration [27], however, very challenging for more detailed characteristics.

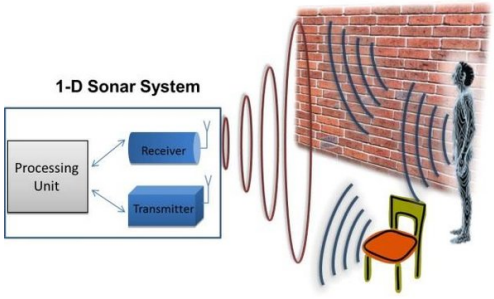

Figure 7: Indoor sonar system where red circles represent the transmitted spherical wave, and the blue curves the returning waves from the objects [24].

3.1.6 Microphone

A baby monitor is commonly used to observe a child from a distance. It records the sounds at the baby's end and plays it back at the receiving end, usually the parents/guardians. The recording end of such a system can also be used to provide data for an algorithm that examines the presence of a baby. But the remaining question is then how the algorithm would distinguish the baby's sound from other ambient noises.
A way to examine the presence of a person would be to detect the breathing pattern [28]. An algorithm can detect a pattern in the measured peaks. However, the sound that a breathing movement induces, results in a signal with very low power, and would be very sensitive to noise (e.g. another car driving by in our situation).
Although it is easy for parents/guardians to examine the presence of a child when listening to the sounds of the child, it is hard for an algorithm to distinguish whether the sound was caused by a child or just a car driving by.
Respiration and even heartbeat with very little ambient noise are possible to detect using a microphone, however, ambient noise can overshadow the signal very fast.

3.2 Contact-based technologies

3.2.1 Piezoresistive sensor

Piezoresistive sensors rely on piezoresistors. Piezoresistors have a resistance as a function of applied pressure. The resistors can be implemented in a t-shirt or blanket which is in direct contact with the baby. The breathing information is directly embedded in the resistance value, which can be read out with for example a Wheatstone bridge. A simple example of how to evaluate certain performance aspects of vital sign detection using piezoresistors is given in Appendix A.1.
The advantages of a piezoresistor are low cost, low power, use very little data and weather independent performance. The big disadvantage is the implementation, which requires contact with the human.

3.2.2 Piezoelectric sensors

A piezoelectric sensor is a crystal that is randomly polarized when no external force is applied. The sensor experiences a force when the chest is pushing against the piezoelectric sensor while a human is breathing in. This will align all the dipoles in the crystal and generates an induced voltage that can be measured. When breathing out, the force of the chest pushing against the piezoelectric sensor is changing and therefore also the induced voltage. This difference in voltage can be used to extract information about respiration rate.
A big advantage of piezoelectric sensors is that they are considered as active sensors, as there is no supply source needed to get an induced output voltage [29]. Advantages of piezoelectric sensors are that they are small, low cost [30], weather independent and can also detect other human vital signs such as heartbeat. An advantage of a piezoelectric sensor over an piezoresistive sensor is that it does not need a measuring circuit such as a Wheatstone bridge and does not need a supply source. The data usage would be comparable to piezoresistive sensors.
A big disadvantage is that the sensor needs to touch the humans chest, which requires some sort of smart shirt or even a smart seat belt just as the case with piezoelectric sensors.

3.3 Analysis recommendation

A few technologies had disadvantages that were a deal breaker for the purpose of this project. **Piezoelectric** and **Piezoresistive** sensors look very promising. The major drawback is the need of contact between sensor and user. This eliminates piezoelectric and piezoresistive sensors from further investigated in this project.

Radar looks very promising because of its low cost, low power, wireless, weather independent and is also able to detect heartbeat. Because radar is able to detect heartbeat, it is also a good candidate for more advanced situations, which will likely happen in the future.

Infrared has one drawback, which is the dependency of the temperature difference between the observed object and the background temperature. If this dependency can be managed, this technique can be very promising. It is recommended to further investigate infrared.

Optical cameras based on visible light are a viable option, it is a reliable technology that that creates high quality data which can be used for many things, including detecting vital signs. Using this technology would need caution when it comes to privacy compliance. Another drawback is that it is very dependent on ambient light. It is recommended to further investigate optical cameras.

Visible light sensing would be a good option during the day, however, since it is very dependent on ambient light, which is not controllable inside a car, it is not recommended to further investigate this technique.

Sonar, due to the independence of light and vision conditions, is very promising for tracking large human motions, and when a high precision is reached, also for respiration, however, can be challenging to obtain more detailed information. It is recommended to further investigate sonar.

Microphones seem to be a good way to examine the presence of a child when the responsible person is actively involved. However, it is very hard to determine the presence when the system is meant to be operating autonomously. It is not recommended to further investigate the detection with microphones.

4 Radar

This chapter starts with giving a theoretical background of how radar theory could be applied to detect respiration in a received signal in subsections 4.1 and 4.2. Section 4.2.5 will discuss a wave simulation based on numerical methods. The XeThru radar system and its performance will be discussed in section 4.4.

4.1 Physical information of heartbeat and respiration

Consider a radar system using one antenna, approximated as a single point in space at $D_0 = (X_0, Y_0, Z_0)$. A baby's left side of the chest is located in direct line of sight and is approximated as a single stationary point at the origin. This simplified model is shown in Figure 8. D_0 is assumed to be in a region of high directivity of the antenna. The only movement that the baby makes is the expansion and contraction of the abdomen and chest due to heartbeat and respiration. The expansion and contraction is approximated to be only frontal with respect to the baby and may cause a small difference in distance between the radar. This distance is denoted as $\vec{D}[x(t), y(t), z(t)]$ and is dependent on the orientation of the baby.
For convenience, spherical coordinates are used as can be seen in Figure 8. The point of interest is now at (r, θ, ϕ) The angles ϕ and θ are considered to be constant.

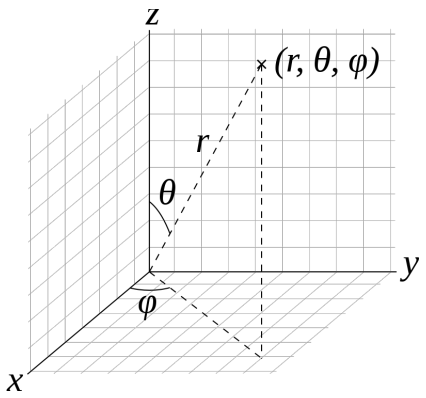

Figure 8: Spherical coordinate system to visualize distance vector[31]

It is assumed that both the baby's respiration and heartbeat frequency, f_r and f_h are constant. Where the subscriptions r and h correspond to respiration and heartbeat respectively.
The same applies for the amplitudes, D_r and D_h, which represent the magnitude of chest displacement. The distance $\vec{D}[x(t), y(t), z(t)]$ is now defined as

$$\begin{aligned} \vec{D}[x(t), y(t), z(t)] &= D_x(t)\hat{x} + D_y(t)\hat{y} + D_z(t)\hat{z} \\ D_x(t) = X_0 + X_r(t) + X_b(t) &= X_0 + [D_r cos(2\pi f_r t) + D_h cos(2\pi f_h t)]cos(\phi)sin(\theta) \\ D_y(t) = Y_0 + Y_r(t) + Y_b(t) &= Y_0 + [D_b cos(2\pi f_b t) + D_h cos(2\pi f_h t)]sin(\phi)sin(\theta) \\ D_z(t) = Z_0 + Z_r(t) + Z_b(t) &= Z_0 + [D_b cos(2\pi f_b t) + D_h cos(2\pi f_h t)]cos(\theta) \end{aligned} \tag{1}$$

The length of $\vec{D}(x, y, z)$ is

$$||\vec{D}[x(t), y(t), z(t)]|| = \sqrt{D_x^2(t) + D_y^2(t) + D_z^2(t)} = r(t) \tag{2}$$

Equation 1 can be simplified to a scalar equation when the baby's chest and abdomen is oriented towards the antenna. This distance, denoted as $D(t)$ is described as

$$D(t) = D_0 + D_r cos(2\pi f_r t) + D_h cos(2\pi f_h t) \tag{3}$$

with D_0 the static distance between antenna and baby.
The rest of this chapter assumes that the baby is directly oriented to the antenna such that the distance is described by Equation 3. $D(t)$ contains information about respiration and heartbeat, however, they are superimposed within the measured $D(t)$. The frequency of respiration and heartbeat are in the order of $[0.3, 1.13]$ and $[1.5, 3.08]$ Hz respectively [32]. We are only interested in the order of magnitude of the respiration and heartbeat frequencies and amplitudes. Using the amplitudes of adults and scaling it down linearly with length, a quick (simplified) approximation was made for babies. The amplitude of respiration and heartbeat are in the range of $[0.86, 4.4]$ and $[0.086, 0.32]$ millimeter respectively. A plot of $D(t)$ is shown in the left plot of Figure 9 where $D_0 = 0.5$, $D_r = 0.002$, $D_h = 0.0002$, $f_r = 0.6$ and $f_h = 2$. A distance of 50 cm as D_0 is used.

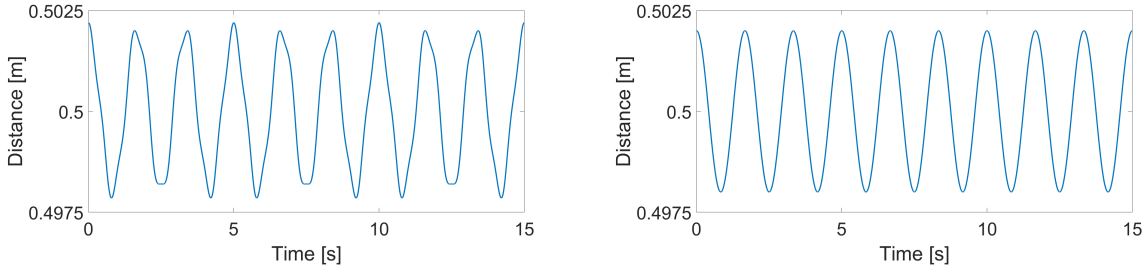

Figure 9: Left: Distance with respiration and heartbeat. Right: Distance with respiration

Detecting heartbeat with radar is very difficult due to a small D_h. Therefore, we simplify the situation by neglecting the heartbeat. The new $D(t)$ can be seen in the right plot of Figure 9. This assumption simplifies equation 3 into

$$D(t) = D_0 + D_r cos(2\pi f_r t) \tag{4}$$

and $\frac{dD(t)}{dt}$, the velocity, becomes

$$\frac{dD(t)}{dt} = -2\pi f_r D_r sin(2\pi f_r t) \tag{5}$$

4.2 Detecting respiration

The movement of the chest and abdomen due to respiration causes a periodic change in $D(t)$ over time. This implies that information about $D(t)$ or $\frac{dD(t)}{dt}$ from Equations 4 and 5 give information about the respiration and heartbeat.
There are many approaches to detect $D(t)$ and $\frac{dD(t)}{dt}$. However, we will consider the following:

- Measurement of the Doppler frequency to estimate $\frac{dD(t)}{dt}$
- Measurement of the round-trip delay to estimate $D(t)$
- Measurement of the frequency difference due to frequency modulation to estimate $D(t)$

This section will show how the information of respiration is stored in the received signal.

4.2.1 Doppler shift using continuous wave radar

This section describes how a frequency difference, a Doppler shift, due to a change of $D(t)$ can lead to the detection of respiration. A simplified block diagram of needed steps are give in Figure 10.

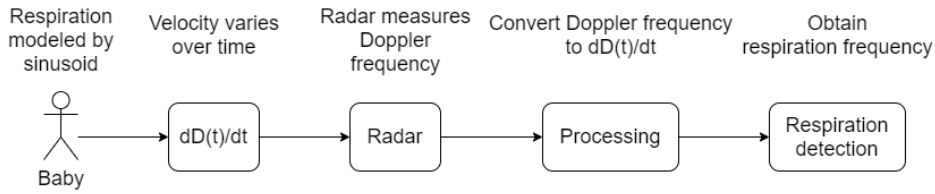

Figure 10: Block diagram of the detection of $D(t)$ through Doppler frequency measurement

Consider transmitting a signal $s(t) = A_t cos(2\pi f_c t)$, from the antenna to the baby. $s(t)$ will return at the antenna with a frequency dependent of the change of distance over time $\frac{dD(t)}{dt}$. The received signal, $s_r(t)$, can be described using the Doppler effect

$$s_r(t) = A_r cos\{2\pi f_c[1 - \frac{2\frac{dD(t)}{dt}}{c}]t\} = A_r cos[2\pi(f_c + f_D)t] \tag{6}$$

with f_c the carrier frequency. This implies that the Doppler frequency is given as

$$f_D = \frac{-2f_c\frac{dD(t)}{dt}}{c} \tag{7}$$

The minus term in Equation 7 illustrates how an increasing distance results in a negative Doppler frequency and vice versa.

4.2.2 Time delay with pulsed radar

A method to obtain $D(t)$ is to measure the round-trip time T_R, which is related to $D(t)$ as

$$D(t) = \frac{cT_R}{2} \tag{8}$$

with c the speed of light. A simplified block diagram of the process can be seen in Figure 11.

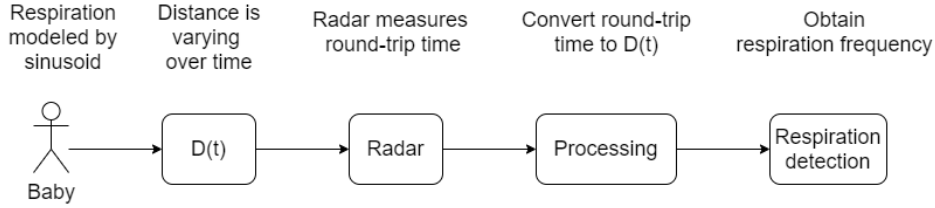

Figure 11: Simplified block diagram of the detection of $D(t)$ through round-trip time

T_R is measured by counting the number of clock pulses passed between transmitting and receiving. To connect T_R with the corresponding transmitted signal, there is an alternation

between transmitting and receiving, called pulsed radar. Pulsed radar can be seen as a form of amplitude modulation and can be modulated as

$$s(t) = A_t[1 + m(t)]cos(2\pi f_c t) \tag{9}$$

with m(t) a periodic signal with period T. $m(t)$ is the modulation index, defined as

$$m(t) = \begin{cases} 0, & \text{if } kT \leq t \leq kT + \tau, \quad 0 \leq \tau \leq T \\ -1, & \text{otherwise} \end{cases} \tag{10}$$

with k a whole number. When τ is chosen such that $\tau \ll T$, the interval $\Big(kT+\tau, (k+1)T\Big)$ can be used to listen for an echo. When $T_R < T$, $D(t)$ can be determined unambiguously. However, one has to deal with multi-path propagation using this type of signal when estimation is desired.

4.2.3 Doppler shift using pulsed radar

Measuring the Doppler frequency with a pulsed radar gives the same block diagram as with continuous wave, as can be seen in Figure 10.
In practice, τ is chosen such that $\tau \ll T$. This requires that the transmitted signal from Equation 9 to be sampled over multiple periods T, with sample period τ. The received signal, sampled at time instances $k\tau$, with both k and n as positive integers, is described by

$$s_r(k\tau) = \begin{cases} A_r[1 + m(k\tau)]cos[2\pi(f_c + f_D)k\tau], & \text{if } nT \leq k\tau \leq nT + \tau, \quad 0 \leq \tau \leq T \\ 0, & \text{otherwise} \end{cases} \tag{11}$$

4.2.4 Time delay using FMCW radar

An alternative to pulsed radar to measure T_R is to modulate the carrier frequency. The block diagram to detect respiration through a frequency modulated signal can be seen in Figure 12.

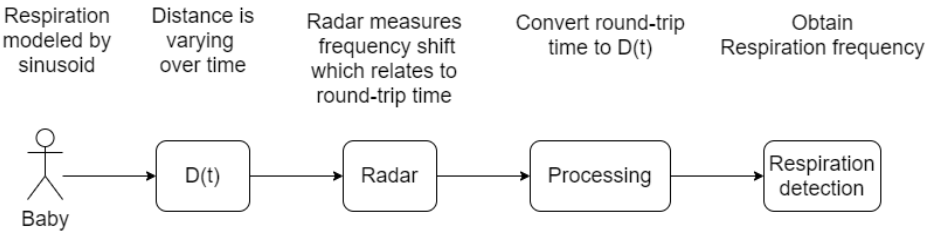

Figure 12: Simplified block diagram of the detection of D(t) through frequency difference

The transmitted signal, called frequency modulated continuous wave (FMCW) can be described as

$$s(t) = A_t cos\{2\pi[f_c + m(t)]t\} \tag{12}$$

With $m(t)$ containing information about when it was sent, assumed that $D(t)$ is smaller than the unambiguous range. The round-trip time can now be determined by controlling the

frequency change over time, $\frac{dm(t)}{dt}$. We will consider a periodically constant $\frac{dm(t)}{dt}$, for example a saw-tooth signal with period T, assuming $T >> T_R$.
The received signal has a different frequency compared with the transmitted signal at that time instant. This difference $|\Delta f|$ is related to T_R provided that $T_R \leq T$, by

$$|\Delta f(t)| = T_R \frac{dm(t)}{dt} + f_D \tag{13}$$

with f_D the Doppler frequency shift, superimposed on $T_R \frac{dm(t)}{dt}$. The absolute signs are to avoid negative T_R. Combining Equations 12 and 13 can give an equation for $D(t)$. The information about respiration is packaged in $|\Delta f|$, which requires an accurate estimation of f_D. However, f_D itself also contains all the information about the respiration frequency. Multi-path propagation has also to be dealt with. Therefore it is far more trivial to use a CW radar instead of a FMCW radar.

4.2.5 Wave simulation

To provide evidence for our reasoning we tried to make a wave propagation simulation in Python. The simulation modeled the two-dimensional wave equation

$$\frac{1}{c^2}\frac{\partial^2 u}{\partial t^2} = \frac{\partial^2 u}{\partial x^2} + \frac{\partial^2 u}{\partial y^2} + f \tag{14}$$

with

- a physical quantity u such as electric field, magnetic field or pressure
- a source function f

Equation 14 is solved by using numerical methods. The time stepping was done by using a finite-difference time-domain approach.
Unfortunately, the simulation came with many challenges and was too time consuming. The simulation was considered as an extra objective to give some more insight, therefore it was decided to stop working on the wave simulation, despite no functioning simulation was achieved. The numerical approach and problems that occurred are explained in appendix B.1.

4.3 XeThru Radar System

For the investigation on the technical aspects of a specific radar system, the XeThru radar system is chosen. This is the system that is planned to implement in the car, and has been used to create data for the Signal Processing group [3]. The test setup used to create this data is described in [33], where experiments of detecting respiration are done.

The XeThru X4M200 is an Ultra Wideband (UWB) short-range impulse radar, used for respiration detection [34]. The respiration experiment done using this radar is based on the radar's high-precision motion detection function to detect the chest undulation to extract the respiration rate. The relative motion between the chest and the radar generates the Doppler effect, described in 4.2.1.

The experiments were done for 20 seconds at distances from 1 to 5 meter from the radar, at different azimuth and zenith angles with respect to the radar direction. The results of the experiments show that the detection of respiration is possible in every tested angle and distances. For some locations that are approaching a chest movement perpendicular to the radar, the detection is difficult and not as clearly measurable, but those regions are not in the scope of our implementation in car, i.e. around 1 meter and a favourable angle.

Figure 13: XeThru X4M200 Respiration Sensor [35]

For the detection of heartbeat, this radar based respiration sensor would not be accurate enough. However, a more advanced XeThru X4 radar will be briefly discussed in Section 4.4.7.

4.4 XeThru Technical Aspects

Given that the X4M200 radar is suitable for respiration detection, the technical aspects of this radar are listed and discussed, with respect to the possibility of implementing the system in a car to detect the respiration of a baby. For the implementation we assume that the radar will be placed at a distance of 1 meter in front of the chest of the baby.

4.4.1 Accuracy

Respiration movement ranges from 4–12 mm with a frequency range of 0.1–0.34 Hz. The frequency resolution of the data is dependent on the number of samples from the measurement that you use for the Fast Fourier Transform (FFT). A moving target is observed for a total time, that time is the product of the duration of a single radar waveform T and the number of waveforms N collected in that time. The Doppler resolution is the inverse of that product, so 1/(NT). This means that the resolution is completely determined by the total observed time, since you can not set N or T arbitrarily. Hence, to achieve an accuracy of at least 0.1 Hz to detect respiration, the observation time should be at least 10 seconds.

When considering the estimation of the respiration rate, which can be extracted in the frequency domain of the recorded data using the FFT on the data, the same approach would be applicable for the resolution of the respiration signals, but will be expressed in an accuracy in terms of respirations per minute (RPM). When assuming that the FFT is computed with the minimum 10 second window, this gives a frequency resolution of 1/10 Hz = 0.1 Hz * 60 sec = 6 RPM. With a longer observation time, or some more desired extra filtering and signal reconstruction, this resolution can be improved further.

4.4.2 Reliability

When assuming that the baby is in front of the radar at a 1 meter distance, using the minimum observing time of 10 seconds, the respiration of the baby is reliably detected at all times. Some difficulties might arise when the baby would be at different angles with respect to the radar. In the case that a baby would be perpendicular to the radar, the respiration signal might not

be strong enough anymore to be detected. A radar system based on multipath would be a future solution to that.
Furthermore, if we want to expand to a system where one radar would be used to detect multiple babies, some more problems will arise. If more than one person is present in the detection zone, the X4M200 sensor is designed to measure the one who is closest to the sensor. This would be sufficient for triggering an alarm when at least one baby is in the car. However, when we want to detect both the respiration rates, a second radar would be necessary. If the babies would be at the same distance, one radar system can not distinguish the signals and they would interfere.

4.4.3 Power Consumption

The power consumption of the XeThru X4M200 is expected around 600 mW, according to the datasheet [35], with a supply voltage of 3.3-5.5 V. All the necessary hardware is present on the module. An external power supply such as a battery can be used.

4.4.4 Dimensions

The dimensions of the module are 30.4x67.6x7.2 mm. These dimensions are small and quite favourable to implement in the car without many inconvenience.

4.4.5 Complexity

The XeThru X4M200 is a quite simple sensor purely designed for the detection of respiration. Everything that is needed to acquire the respiration rate is present on the module. When heartbeat detection is preferred, a more complex module would be necessary for more accurate measurements.

4.4.6 Costs

The costs of a single XeThru X4M200 Respiration Sensor are €220.00, however, in large quantities the price becomes €70 each/1,000 for the X4M200 Respiration Sensor. This is relatively cheap, since the module includes everything that is needed, except for a power supply.

4.4.7 Heartbeat detection

With the XeThru X4M200 radar that is discussed for the investigation in respiration detection, heartbeat detection would not seem possible. However, a more advanced XeThru radar, the X4M06, has been proven to be able to detect heartbeat [36]. The current state of these radars would not be suitable for the detection of heartbeat inside a car. The experiments were done under very simplified During the measurement, participants were told to hold their breath for 15-20. This way, the respiration movement of the chest would not influence the measurement, however, 10 seconds of the data could be used as it would even take a few seconds for the radar device to acquire clear data without respiratory noise after the participant started holding their breath. This experiment was done to investigate whether radar can detect artrial fibrillation (AF), a cardiac arrhythmia, compared to electrocardiogram (ECG) technology, primarily used for diagnosing atrial fibrillation.

5 Infrared thermography and Optical RGB cameras

5.1 Why this system?

The detection of people has been done using either infrared thermography (IRT) or optical RGB cameras separately. Both of these technologies have their pros and cons, IRT does not depend on different light circumstances, while optical RGB cameras do. On the other hand, IRT measurements are influenced by environmental temperature and humidity, which do not have an effect on RGB cameras. Therefore, an existing system that combines both technologies is considered for the application in a car, so the benefits of both technologies can be highlighted, while filtering out their drawbacks. In addition to that, state of the art systems to investigate breathing rate and heartbeat measurements based on infrared light still rely on the facial recognition by optical cameras. Hence, in this chapter, the two technologies will be discussed together.
The system that is considered to investigate its possibilities for implementation in a car is originally used to remotely sense a deviation in breathing rate, heart rate and body temperature to screen patients with suspected infectious diseases [37] [38].

5.2 How does the system work?

The system consists of a CMOS Camera that is equipped with a thermal imager (TVS-500; NEC/AVIO Infrared Technologies Co. Ltd, Tokyo, Japan) to extract the above mentioned vital signs from facial images [37]. Figure 14 gives an overview of the methods of the system, consisting of:

- Breathing detection using infrared thermography
- Heartbeat detection using an optical RGB camera

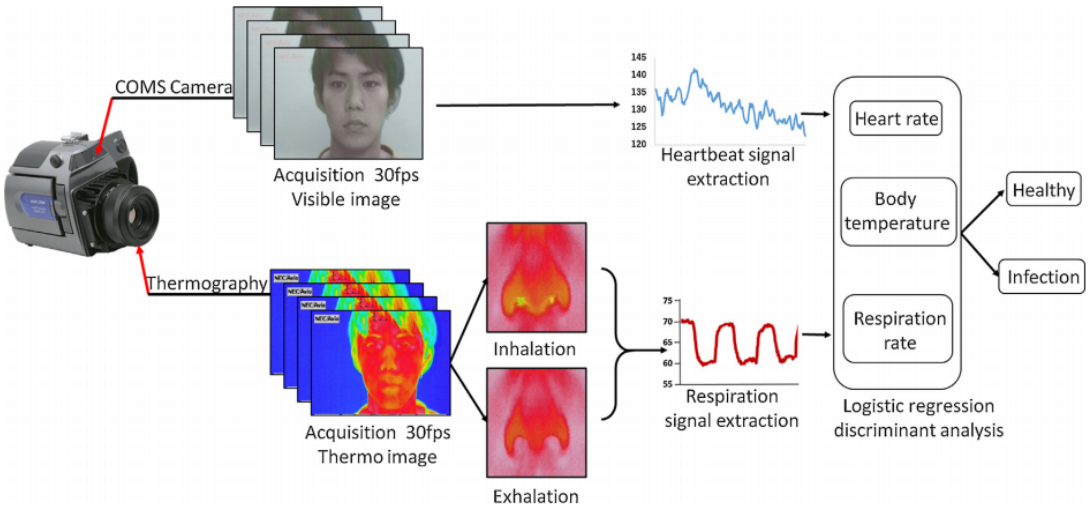

Figure 14: Schematic representation of the visible and thermal image processing method that remotely senses multiple vital signs and the multiple logistic regression function that predicts the possibility of infection. [37]

The breathing rate can be detected and estimated by monitoring the temperature changes around the nasal and oral areas accompanying inspiration and expiration, IRT is used to measure these changes in temperature. The RGB camera measures the blood volume pulse (BVP) through variations in the light absorption from the human facial area, to detect and estimate heartbeat.
It is worth mentioning that both breathing and heartbeat can be detected and estimated using upcoming advanced IRT systems, but there is still very few research done on those systems [39]. However, when these systems improve, at some point they will outperform optical cameras for heartbeat detection, as optical cameras are still dependent of ambient light. For our research, we stick to the commonly used CMOS camera-equipped IRT system.

5.3 Region of Interest

The measurements in the experiments are performed at a distance of 0.5 to 1 meter between the camera and the human face. For a stable detection of the respiration rate and heart rate, before extracting any data from the images, a detailed region of interest (ROI) in the measurement is needed, this is done by the detection of facial landmarks (i.e., nose and mouth), as respiration occurs at the nose and mouth. For visible images from RGB cameras, there are many methods to track human faces [40]. To obtain the same facial coordinates in the thermal image, a sensor fusion methods is used, based on the homography between the images.

5.3.1 Infrared Thermography

To measure the respiration rate from the thermal images, the temperature changes that occur around the nasal and oral area during the inspiration of cold air from the environment and the expiration of warm air from the lungs are monitored, and the respiratory waveform is extracted from the differences in each of the thermal images. This enables the respiration rate to be determined from the breath-to-breath intervals. How the respiration rate is extracted from the thermal video is elaborated in Appendix C.1.

5.3.2 CMOS Camera

An optical camera can be used for non-contact measurement of respiration rate and heart rate via image processing [41]. The involved technique to detect heart rate is based on the photoplethysmograph (PPG), which can detect the blood volume variation by analyzing the transmitted or reacted light. During the cardiac cycle, volumetric changes in the facial blood vessels modify the path length of the incident ambient light such that the subsequent changes in amount of reflected light indicate the timing of cardiovascular events. How the heartbeat is detected and estimated using optical cameras is elaborated in-depth in Appendix C.2. An optical camera can also be used to detect the breathing rate, by measuring the movement of the chest.

5.4 Technical Aspects

We can conclude that infrared and optical cameras are a suitable option for breathing detection, and even the estimation of the breathing rate and heart rate. In this section, the

possibility of implementing such a system in a car is discussed on the basis of their technical aspects.

5.4.1 Accuracy

The accuracy of this system depends on the accuracy of the camera and the performance of the signal processing. The accuracy of the camera would be the most critical for the system in our car, when only breathing detection is considered. The CMOS-IR camera has a temperature resolution better than 0.05°C in the range of -40 to 500°C with an accuracy ±2%. This is sufficient to detect the temperature differences between inhaling and exhaling, and the environmental temperature.
The optical camera has a resolution of 640x480 pixels and a frame time of 1/60 seconds. This is accurate enough to detect the average heartbeat of 1 - 1.8 Hz (frame rate high enough), on the basis of the changes in amount of reflected light in facial blood vessels (enough pixels to see blood vessels with a mean diameter of around 2.7 mm [42]). More complex signal processing or a better camera resolution can be used to improve to future estimation of the breathing rate and heart rate.

In the experiments, the accuracy of the system was determined by whether the detector could indicate if a person was healthy or not. This was based on an measurements with a 95% limit of agreement range in the Band-Altman plots of [-10.4, 12.6] bpm and [-2.97, 3.67] bpm for heartbeat and respiration rate respectively. The standard deviation for the heart was 5.85 for the heart rate and 1.68 for the respiration rate. This would be marginally accurate for the main goal of our system, to detect the breathing of a baby. An extension to heartbeat detection, and even the estimation of both is possible.

5.4.2 Reliability

Several major aspects that have a noticeable influence on the reliability of the system when implementing it in a car are:

- the measurement distance,
- the operational temperature,
- the field of view (FOV) of the camera.

The measurement distance of the camera the is used is listed at 30 cm to infinity, given that the distance from the camera to the baby will correspond to 0.5 - 1 meter, this is sufficient.
The operational temperature of the camera is -10 to 50°C with a relative humidity of 80% or less. This would rise some problems, as our goal is to prevent being left behind in a car with extraordinary car temperatures of 50 - 70°C. However, the temperature inside a car rises to 50°C in about 30 to 60 minutes, with an outside temperature of 30 to 40°C. Thus, despite it is not favourable, the problem can be managed by a memory in the system to remember that a baby was reliably detected in the first 30 minutes. Estimation would then be out of the scope.

The listed FOV corresponds to 19.4°(H) and 14.6°(V) with the standard 22mm lens. This means that the FOV is 17.1x12.85 cm at a distance of 0.5 meter from the camera, and 34.2x25.7 cm at 1 meter. Such a FOV would require an accurate placement in the car, which

is achievable in the situation of a baby in a baby chair, but would require calibration for different cars and different chairs. For a favourable implementation in a car, the lens could be easily replaced by a bigger one to increase the FOV. When the FOV would be doubled, the FOV per pixel would double from 0.27x0.27 mm to 0.54x0.54 mm, which is still marginally accurate to detect heartbeat.
Another very obvious aspect to consider when a reliable optical heartbeat detection is required at all times, is the influence of ambient light. In the dark, the optical camera would need an external light source to be functional.

5.4.3 Power consumption

The power consumption of the camera is 14 W. With the standard provided battery, the operating time is approximately 2 hours, which is increased to 4 hours when using the optional long life battery. For the stand-alone implementation in a car, the processing will be on sight instead of using a PC. The extra required hardware, a microcontroller consisting of at least a digital signal processor, random accessible memory, flash memory and possibly amplifiers and converters, could be considered to implement with an additional power supply, or can be driven by the existing battery.
Unfortunately, little is known about the battery and the operating voltage of the camera. When we assume that the operating voltage of the camera would be 5 V (12 V Li-ion battery packs are generally quite big, especially considering the size of a camera), the current would be 2.8 A. Although it is also hard to estimate what type of microcontroller would be needed, it is safe to say that the power consumption would be in the order of mW, with a current of a few mA. Thus, the extra hardware could be powered by the existing battery, only reducing the operating time by a small amount. Recalling that the minimum operation time of the system was required to be 2 hours, it can be concluded that the above mentioned long life battery can be used to power the whole implemented system.

5.4.4 Dimensions

The dimensions of the camera are 140(H)x140(W)x226(D) mm including protrusions, with a weight of 1.9 Kg without battery. The required extra hardware would only add a few mm to the total size, and can be placed in the most desirable location for as little inconvenience as possible. These dimensions comply with the required dimensions of the system implementation.

5.4.5 Complexity

Unfortunately, there is very little known (made public) about the hardware of the camera itself. A statement about the software does mention that when a thermal image and visible image was simultaneously created, 7200 rpm or faster 3.5FDD was required, which is of course nothing in today's technologies. Since the camera provides a digital BMP file format, no external ADC is necessary.

5.4.6 Costs

The price of the camera is unknown, since it is a discontinued model. However, thermal imagers tend to rise to a price of several thousands of euros, which is quite expensive.

6 Sonar technology

This chapter will go more in-depth on using a sonar system for detecting human vital signs in a car. Section 6.1 will discuss why this specific system is chosen. Section 6.2 explain how this system works and Section 6.3 will evaluate the performance of the system.

6.1 Why this system

The chosen system is SonarBeat [27]. SonarBeat is able to detect and estimate respiration very accurately, while the system is kept simple to implement. The experiment uses a bedroom environment to estimate breathing of one person, which comes close to a baby left alone in a car.
On the downside, not all features of the smartphone are used, which make this system unnecessary complex.

6.2 How does this system work

The SonarBeat is a system used for detecting of respiration. The SonarBeat consists of a microphone, loudspeaker, a signal generator and a processor capable of signal processing, all implemented in the smartphone. The used smartphones were the Samsung Galaxy S6 and the Samsung Galaxy S7 Edge.
The information of the respiration is hidden in the received phase, which is extracted using arctangent demodulation. A block diagram of the SonarBeat system is given in Figure 15. The SonarBeat system can be decomposed in four blocks:

- Signal Generation, which generates the transmitted CW signal;
- Data Extraction, which is responsible for transmitting and detection of the transmitted signal in the received signal using a STFT;
- Received Signal Preprocessing, which removes static interference using an adaptive median filter and filters out noise, based on arctangent demodulation;
- Breathing Rate Estimation, which estimates the Breathing rate using the FFT.

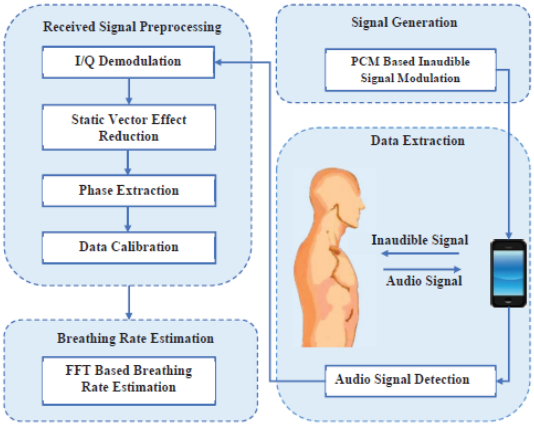

Figure 15: SonarBeat system architecture [27]

6.3 Region of Interest

The region of interest is the same as for radar, the left side of the chest. The distance is assumed to be 0.5 m. No calibration is needed.

6.4 Technical aspects

In this section all technical aspects of the SonarBeat are considered to represent Sonar.

6.4.1 Accuracy

The resolution of sonar is based on the observation time. The respiration frequency range is between $[0.3, 1.13]$ as stated in Section 4.1. To be able to detect this complete range, at least one period of the lowest frequency should be observed.
The SonarBeat observes for 15 seconds which means that a signal as small as 0.0667 Hz can be detected. 0.0667 Hz is small enough to be able to detect all healthy respiration rates.
The resolution can be made arbitrarily small by increasing the observation time, however this will increase the memory usage in the signal processor.
Tests with the SonarBeat gave a maximum estimation error of 2.4 bpm [27]. While 95% of the test results had an estimated error under 0.5 bpm.

6.4.2 Reliability

When the baby is not directly oriented to the loudspeaker and microphone, the detectable Doppler frequency still occurs through multi-path propagation. However, the traveled distance is increased. The energy of the pressure wave is attenuating in air can be read out of an interactive plot [43]. We used a frequency of 20 kHz, a humidity of 48.9% [44], which gives an attenuation of 0.582 dB/m. The distance traveled of acoustic waves between the baby and the smartphone is in the order of several meters in the worst case. This happens when acoustic wave has to be reflected several times on the inside of the car before reaching the region of interest of the baby. This would make the attenuation in the order of dB.
Conclusion, the received signal power of a sonar system in air is depending on the traveled distance, which is depending on the orientation of the baby. However, in the situation of a car, this would be only in the order of dB. which makes the received signal power dependent on the total displacement of the pressure wave. The transmitted power has to be increased to be able to compensate for a possible rotation of the baby.

The operating temperatures limit of both smartphones is based on the CPU. The mandatory requirement of 70°C is in general within the range of operating temperatures of CPU's.

6.4.3 Dimensions

The complete SonarBeat system is integrated in a smartphone. The dimensions of the used smartphones are given below to give an idea about the order of magnitude.
The dimension of the Samsung Galaxy S6 are 143.4(H)×70.5(W)× 6.8(D) mm with a weight of 138g [45].
The dimensions of the Samsung Galaxy S7 Edge are 150.9(H)× 72.6(W)×7.7(D) mm[46].

6.4.4 Power consumption

The battery capacity of the Samsung Galaxy S6 and Samsung Galaxy S7 Edge are 9.82 and 13.86 Wh respectively.
Unfortunately, there is no data available about the power consumption of the SonarBeat. However, research has been done on power consumption of smartphones which showed that using the maximum audio power usage and CPU capacity gives a power consumption range of $[1, 2]$ W [47]. To be safe, we assume that the power usage is 2 W, but is likely much less. Using the drain capacity of the batteries, it can be concluded that the Samsung Galaxy S6 and Samsung Galaxy S7 Edge can sense around 4.91 and 6.93 hours respectively in the worst-case scenario.
If we had had made the SonarBeat ourselves, we would have estimated the power consumption by $\frac{\text{Battery capacity}}{\text{Discharge time}}$.

6.4.5 Complexity

All functions of the SonarBeat system are performed by the smartphone, so there is no extra equipment required.
The upper bound of the memory usage of the SonarBeat system is lower than the working memory of the Samsung Galaxy S6, which is 3 Gb RAM[45]. If we had made the SonarBeat ourselves, the data usage would be obtained by using a profiler. The profiler would tell how much memory is used by the program and tell which parts of the code are using the most memory.

6.4.6 Cost

The price of a new Samsung Galaxy S6 can be found on the internet for around €210, for example at bol.com (www.bol.com). However, due to the unknown power consumption and data complexity, it is possible that a much cheaper smartphone could be used. Especially since the purpose of this project is to detect respiration only, instead of estimation.

6.4.7 Heartbeat detection

Heartbeat can be detected with sonar, but is more challenging than respiration. This is due to the smaller magnitude, lacking of large peaks and stronger harmonic components in the signal [48].
Qian et al (2018) provided evidence for using sonar for heartbeat detection and esitimation. They had a heartbeat estimation with a median error of 0.6 bpm.

7 Comparison and Discussion

This chapter gives a comparison between the radar system described in Chapter 4, the infrared and optical system described in Chapter 5 and the sonar system described in Chapter 6. The comparison is done with respect to radar. The goal of this chapter is to provide evidence for or against the use of radar to detect respiration in a car.

7.1 Relative review

Recalling every technical aspect discussed in the previous in-depth chapters, a final overview is made. In this review, we mainly look at the technologies' possibility to detect breathing, but the possibility of heartbeat detection and the estimation of both are considered and listed as a separate aspect. The performance on the technical aspects are graded for every technology on a relative scale that contains: $--$, $-$, $+/-$, $+$, $++$, where $--$ represents very bad performance and $++$ very good performance, in comparison with the other technologies.

	Radar	**Sonar**	**Infrared**	**Optical**
[1] Accuracy	+	+	++	+/-
[2] Reliability	++	+/-	−	−
[3] Power Consumption	++	++	−	−
[4] Dimensions	+	++	−	−
[5] Complexity	+	+/-	−−	+/-
[6] Costs	+	−	−−	−
[7] Heartbeat	++	++	+	++
[8] Estimation	++	+	+/-	+

1. When we look at accuracy in this row, it is only considering the accuracy regarding the detection of breathing
2. The reliability takes into account how environmental circumstances would influences the system
3. No additional explanation needed
4. Obvious grading, from small to big. Sonar is considered here as only a small part of the smartphone.
5. The complexity is difficult to address, but the reasoning behind the decisions in this row is that optical cameras create large amounts of data compared to the rest. Infrared needs extra signal processing to mix the image with the optical image, and to select the best signals. Sonar is graded average, since it is based on a complex smartphone system, and hard to determine the exact complexity of the sonar system itself. Compared to all other technologies, radar seems quite simple.
6. The cost of the system. This leads to an unreliable grade for sonar because of all the unnecessary functions within a smartphone.
7. The possibility of expanding the system based on this technology to detect heartbeat
8. The possibility of expanding the system based on this technology to make an estimation of the respiration rate and heart rate

7.2 Relative performance of Radar

Looking at Table 7.1, it can be seen that **radar** comes out best. In this section, the biggest considerations which give this final result are discussed.

When we compare radar with **infrared** the biggest downside of infrared would be the extremely high costs. Also, the current state of art of infrared systems would need an extra optical camera to acquire a correct ROI in the thermal image. This is extra hardware and extra signal processing, which is not needed with radar. Although the infrared technology is rising for heartbeat detection, it is still its infancy. Radar has already been proven to detect heartbeat quite accurately for a longer time. Another major drawback of infrared, compared to radar, is that the power consumption of the infrared system turned out to be 10 times as high.

Optical cameras are a great option to detect heartbeat, and can also be used to detect breathing. However, doing both would require two different ROIs (i.e. the chest for breathing and the face for heartbeat). A system based on radar technology does both by measuring in the chest region. While radar is not dependent on any environmental circumstances, an optical camera is sensitive to changes in ambient light, humidity, dust, smoke, etc. Considering the power consumption, the same would hold as for infrared. The power consumption of radar is very low compared to optical cameras.

Sonar is a great option to both detect and estimate respiration and heartbeat. However, the biggest disadvantage of sonar compared to radar is the dependency of the received signal power of on the displacement. When a less complex sonar system is considered, it would be slightly below radar.

8 Conclusion and recommendation

8.1 Conclusion

This thesis started out with an investigation on a large arsenal of technologies that are capable of detecting human presence, with respiration detection kept in mind. As a result of a broad look at many of these technologies, it was found that radar, sonar, infrared and optical cameras were worth further investigation, based on the mandatory requirements.

All four of the further investigated technologies were able to detect respiration and heartbeat. A performance evaluation with respect to radar was then carried out, based on:

- Accuracy
- Reliability
- Power consumption
- Dimensions
- Complexity
- Costs
- Heartbeat
- Estimation

The conclusion, based on the points described above, is that radar is indeed the best choice to detect human presence based on respiration for the implementation in a car. With this technology, babies can be detected inside a car, and saved when they are left behind.

8.2 Recommendation

Due to the fact that all the needed information of the baby can be extracted from the velocity of the chest, it is recommended to further investigate a radar system that makes use of the Doppler effect, instead of range. A system based on this distance is more sensitive to multi-path propagation issues.
We recommend to investigate further in both CW and pulsed radar. However, a big concern would be the direct-path between the transmitter and the sensitive receiver. We recommend to investigate the use of a circulator to prevent this direct-path or consider separate antennas for the transmitter and receiver.

References

[1] J. Booth, G. Davis, J. Waterbor, and G. Mcgwin, "Hyperthermia deaths among children in parked vehicles: An analysis of 231 fatalities in the united states, 1999–2007," *Forensic science, medicine, and pathology*, vol. 6, pp. 99–105, 03 2010.

[2] R. Kooij and S. Neji, "Radar based human vital sign detection in cars: A system analysis," 2020.

[3] X.-C. Hsiao and I. Achinuhu, "Radar based human vital sign detection in cars: Signal processing," 2020.

[4] A. P. Sage and J. E. Armstrong, *Introduction to systems engineering*. John Wiley Sons, 2000.

[5] R. E. Weiss, *Convertible Car Seat*. Verywell Family, May 2020. [Online]. Available: https://www.verywellfamily.com/types-of-baby-car-seats-2758097

[6] Y. Kim, S. Ha, and J. Kwon, "Human detection using doppler radar based on physical characteristics of targets," *Geoscience and Remote Sensing Letters, IEEE*, vol. 12, pp. 289–293, 01 2015.

[7] M. Rabbani and H. Ghafouri-Shiraz, "Ultra-wide patch antenna array design at 60 ghz band for remote vital sign monitoring with doppler radar principle," *Journal of Infrared, Millimeter, and Terahertz Waves*, pp. 1–19, 11 2016.

[8] M. Chojnowski, "Infrared thermal imaging in connective tissue diseases," *Reumatologia*, vol. 55, pp. 38–43, 03 2017.

[9] D. Formenti, N. Ludwig, M. Gargano, M. Gondola, N. Dellerma, A. Caumo, and G. Alberti, "Thermal imaging of exercise-associated skin temperature changes in trained and untrained female subjects," *Annals of biomedical engineering*, vol. 41, 12 2012.

[10] G. Tanda, "The use of infrared thermography to detect the skin temperature response to physical activity," vol. 655, 06 2015.

[11] E. Goubet, J. Katz, and F. Porikli, "Pedestrian tracking using thermal infrared imaging - art. no. 62062c," *Proceedings of SPIE 2006, 6206*, vol. 6206, pp. 79–, 06 2006.

[12] P. Goyal, "Review of infrared signal processing algorithms," vol. 2, pp. 176–180, 06 2011.

[13] A. Procházka, H. Charvátová, O. Vyšata, J. Kopal, and J. Chambers, "Breathing analysis using thermal and depth imaging camera video records," *Sensors*, vol. 17, pp. 1408–1, 06 2017.

[14] I. Dadour, I. Almanjahie, N. Fowkes, G. Keady, and K. Vijayan, "Temperature variations in a parked vehicle," *Forensic science international*, vol. 207, pp. 205–11, 11 2010.

[15] A. Fernández-Caballero, M. López Bonal, and J. serrano Cuerda, "Thermal-infrared pedestrian roi extraction through thermal and motion information fusion," *Sensors (Basel, Switzerland)*, vol. 14, pp. 6666–6676, 04 2014.

[16] A. Bovik, "Handbook of image & video processing," 01 2010.

[17] K. Ghazali, W. W. Samsudin, and N. Mohamad Hamid, "Motion detection for pc based on security system by using optical flow," *International Journal on Advanced Science, Engineering and Information Technology*, vol. 2, 12 2011.

[18] R. LUKAC and K. Plataniotis, "Single-sensor camera image processing," 10 2006.

[19] C. Antink, S. Lyra, M. Paul, X. Yu, and S. Leonhardt, "A broader look: Camera-based vital sign estimation across the spectrum," *Yearbook of Medical Informatics*, vol. 28, pp. 102–114, 08 2019.

[20] G. Blumrosen, B. Hod, T. Anker, D. Dolev, and B. Rubinsky, "Enhanced calibration technique for rssi-based ranging in body area networks," *Ad Hoc Networks*, vol. 11, p. 555–569, 01 2013.

[21] A. Kanaujia, N. Haering, G. Taylor, and C. Bregler, "3d human pose and shape estimation from multi-view imagery," *IEEE Computer Society Conference on Computer Vision and Pattern Recognition Workshops*, pp. 49–56, 06 2011.

[22] P. Kelly, S. Marshall, H. Badland, J. Kerr, M. Smith, A. Doherty, and C. Foster, "An ethical framework for automated, wearable cameras in health behavior research," *American journal of preventive medicine*, vol. 44, pp. 314–9, 03 2013.

[23] H. Abuella and S. Ekin, "Non-contact vital signs monitoring through visible light sensing," *IEEE Sensors Journal*, vol. PP, pp. 1–1, 12 2019.

[24] G. Blumrosen, B. Fishman, and Y. Yovel, "Non-contact wideband sonar for human activity detection and classification," *IEEE Sensors Journal*, vol. 14, 08 2014.

[25] J. Sabatier and A. Ekimov, "Ultrasonic methods for human motion detection," 04 2008.

[26] Z. Zhang, P. Pouliquen, A. Waxman, and A. Andreou, "Acoustic micro-doppler gait signatures of humans and animals," 04 2007, pp. 627 – 630.

[27] X. Wang, R. Huang, and S. Mao, "Sonarbeat: Sonar phase for breathing beat monitoring with smartphones," 09 2017, pp. 1–2.

[28] E. Ziganshin, M. Numerov, and S. Vygolov, "Uwb baby monitor," 10 2010, pp. 159 – 161.

[29] G. Gautschi, *Piezoelectric Sensors*, 01 2002, pp. 73–91.

[30] A. Rasheed, E. Iranmanesh, W. Li, Y. Xu, Q. Zhou, H. Ou, and K. Wang, "An active self-driven piezoelectric sensor enabling real-time respiration monitoring," *Sensors*, vol. 19, p. 3241, 07 2019.

[31] "Vector fields in cylindrical and spherical coordinates," June 2020. [Online]. Available: https://en.wikipedia.org/wiki/Vector_fields_in_cylindrical_and_spherical_coordinates

[32] S. Fleming, M. Thompson, R. Stevens, C. Heneghan, A. Plüddemann, I. Maconochie, L. Tarassenko, and D. Mant, "Normal ranges of heart rate and respiratory rate in children from birth to 18 years of age: A systematic review of observational studies," *Lancet*, vol. 377, pp. 1011–8, 03 2011.

[33] J. Peng, "Assessment capabilities of short-ranged commercial radar sensors," 2018.

[34] "Ultra wideband (uwb) impulse radar transceiver soc," Novelda, 3 2020, rev. F.

[35] "Respiration sensor," Novelda, 12 2017, rev. C.

[36] Y. Lee, J. Park, Y. Choi, H. Park, S. Cho, S. Cho, and Y. Lim, "A novel non-contact heart rate monitor using impulse-radio ultra-wideband (ir-uwb) radar technology," *Scientific Reports*, vol. 8, no. 1, Dec. 2018.

[37] G. Sun, Y. Nakayama, S. Dagdanpurev, S. Abe, H. Nishimura, T. Kirimoto, and T. Matsui, "Remote sensing of multiple vital signs using a cmos camera-equipped infrared thermography system and its clinical application in rapidly screening patients with suspected infectious diseases," *International Journal of Infectious Diseases*, vol. 55, 01 2017.

[38] T. Negishi, S. Abe, T. Matsui, H. Liu, M. Kurosawa, T. Kirimoto, and G. Sun, "Contactless vital signs measurement system using rgb-thermal image sensors and its clinical screening test on patients with seasonal influenza," *Sensors*, vol. 20, p. 2171, 04 2020.

[39] Q. Zhang, Y. Zhou, S. Song, G. Liang, and H. Ni, "Heart rate extraction based on near-infrared camera: Towards driver state monitoring," *IEEE Access*, vol. PP, pp. 1–1, 06 2018.

[40] G. R. Bradski, "Real time face and object tracking as a component of a perceptual user interface," in *Proceedings Fourth IEEE Workshop on Applications of Computer Vision. WACV'98 (Cat. No.98EX201)*, 1998, pp. 214–219.

[41] M.-Z. Poh, D. McDuff, and R. Picard, "Advancements in noncontact, multiparameter physiological measurements using a webcam," *IEEE transactions on bio-medical engineering*, vol. 58, pp. 7–11, 10 2010.

[42] O. Magden, M. Edizer, V. Tayfur, and A. Atabey, "Anatomic study of the vasculature of the submental artery flap," *Plastic and reconstructive surgery*, vol. 114, pp. 1719–23, 01 2005.

[43] D. Russell, "Acoustics and vibration animations," Dec 2013. [Online]. Available: https://www.acs.psu.edu/drussell/Demos/Absorption/Absorption.html

[44] K. Gładyszewska-Fiedoruk and T. J. Teleszewski, "Modeling of humidity in passenger cars equipped with mechanical ventilation," 06 2020.

[45] "Mobile phones: Android galaxy phones: Samsung us." [Online]. Available: https://www.samsung.com/global/galaxy/galaxys6/galaxy-s6/#!/spec

[46] "Mobile phones: Android galaxy phones: Samsung us." [Online]. Available: https://www.samsung.com/global/galaxy/galaxy-s7/#!/spec

[47] A. Carroll and G. Heiser, "An analysis of power consumption in a smartphone," 2010.

[48] K. Qian, C. Wu, F. Xiao, Y. Zheng, Y. Zhang, Z. Yang, and Y. Liu, "Acousticcardiogram: Monitoring heartbeats using acoustic signals on smart devices," 04 2018, pp. 1574–1582.

[49] E. Vanegas, R. Igual, and I. Plaza, "Piezoresistive breathing sensing system with 3d printed wearable casing," *Journal of Sensors*, vol. 2019, pp. 1–19, 12 2019.

[50] M. Hesse, P. Christ, T. Hörmann, and U. Rückert, "A respiration sensor for a chest-strap based wireless body sensor," vol. 2014, 09 2014.

[51] D. de rossi, F. Carpi, F. Lorussi, A. Mazzoldi, R. Paradiso, E. Scilingo, A. Tognetti, and Smartex, "Electroactive fabrics and wearable biomonitoring devices," *Autex Res. J.*, vol. 3, 11 2002.

[52] N. V. Budko, "Lecture 9, tw3730tu: Wave equation, method-of-lines solution, three-point time-stepping scheme, approximation of initial conditions, cfl stability condition," Jun 2020.

[53] W. Wang, A. C. den Brinker, and G. de Haan, "Single-element remote-ppg," *IEEE Transactions on Biomedical Engineering*, vol. 66, no. 7, pp. 2032–2043, 2019.

Appendices

A Appendix A

A.1 Piezoresistive sensors

Because the Piezoresistive sensor needs an additional measuring circuit, the analysis is done a bit more detailed, such that parameters as power and data usage can be given a quick estimation. In (Ulaby, 1999) a piezoresistive sensor is described which can be applied to measure human breathing. When the chest expands due to breathing in, there will be an increased force experienced by the piezoresistive sensor. This force will stretch the piezoresistor. This stretch will increase the length and simultaneously decrease the cross-sectional area. These geometric changes of the piezoresistor change its resistance. According to (Ulaby, 1999), the relationship between the force and the deviation of the resistance can be approximated by

$$R = R_0 + R_0 \frac{\alpha F}{A_0} \tag{15}$$

Where R_0 and A_0 correspond to the resistance and area when there is no force on the resistor. α is a material property known as the piezoresistive coefficient, which is dimensionless. The deviation of the resistance is caused by the $R_0 \frac{\alpha F}{A_0}$ part. This deviation in resistance is denoted as ΔR and can be easily measured by a Wheatstone bridge circuit, where the output voltage is given by

$$\frac{V_0 \Delta R}{4R_0} = \frac{\alpha F V_0}{4A_0} \tag{16}$$

Where one of the four resistors is a piezoresistor with resistance $R_0 + \Delta R$ instead of R_0. So there is now a direct relation between the applied force on the piezoresistor and the measured voltage. Research shows that the piezoresistance changes during breathing in and breathing out. Only the data of (Vangeas et al, 2019) while sitting down is considered because of the context of inside a vehicle.

In the most simple case, it is enough to quantize the signal with two bits. In this case there is only a distinction between the voltage corresponding to the unstressed resistance, and the voltages corresponding to breathing in and breathing out resistances.

Research shows that the ratio $\frac{\Delta R}{R_0}$ varies roughly between $0.8 - 1.2$ during deep breathing, which happens often during hyperventilation, and $0.9 - 1.1$ during normal breathing[49]. The corresponding output voltages are given in table 2. If only a binary distinction between breathing in and out is made, a treshold of the measured voltage of $0.25V_0$ would distinct breathing in and breathing out for both cases. However, the information between normal and deep breathing is lost.

When the information to distinct between normal and deep breathing should be kept, the quantizer becomes a bit more involved. There are now two main concerns on quantization, the first one is to have a sufficient range to be able to quantify the incoming signal in all desired categories. The largest value according to table 2 is $0.3V_0$. Using $0.3V_0$ as upper input range R, minimizes the range of not used quantization levels.

The second concern is regarding the close spacing between normal and deep breathing in and normal and deep breathing out. Sufficient bits should be used such that the amplitude jump between quantization levels, Δ, is sufficiently low. This jump should be lower than half of

Breathing	Normal	Deep
In	$0.275V_0$	$0.3V_0$
Out	$0.225V_0$	$0.2V_0$

Table 2: Output voltages corresponding to breathing

the distance between any of the four categories. A first approach is to use a linear quantizer to calculate the minimum number of bits required. For a linear quantizer Δ is defined as $\Delta = \frac{R}{2^{b+1}}$. With R the allowed input range and b the number of bits required. Δ should be smaller than $0.025V_0$, $R = 0.3V_0$ and solving for b gives $b \geq 3$. A typical sampling rate used in similar experiments is $f_s = 100Hz$ [50]. This would require a minimum bit rate of 300bit/s.
The Wheatstone power consumption is

$$P = \frac{V_0^2}{R_{eq}} \tag{17}$$

with R_{eq} the equivalent resistance which equals

$$R_{eq} = \frac{4R_0^2 + 2R_0\Delta R}{4R_0 + \Delta R} \tag{18}$$

Similar experiments used a voltage range of $0.2-2.5$ V. In the worst case, $\Delta R = 0$ and $V_0 = 2.5$ V, this would mean a maximum power consumption of $\frac{4}{R_0}$ W. A typical piezoresistor is in the order of $400k\Omega$.[51] Which would give a maximum power consumption of 15.6 μW.

B Appendix B

B.1 Wave simulation

The approach to simulate wave propagation in space was to first simplify the situation. The first model will model a rectangular grid in 2D with no objects, an isotropic source, zero initial conditions and total reflection. When the first model can describe wave propagation in this situation, the aim is to add new functions to the model one by one. Such as changing the grid to the shape of a car, adding objects, moving objects, boundary conditions for transmission, material dependent speed and different radiation patterns for the source etc.
Unfortunately, problems occurred with respect to adding boundary conditions to implement transmission behaviour and execution time. The wavelength of EM waves in the radar frequency range we are interested in are in the order of millimeter. This will create very large matrices, which will be discussed later. This resulted in stopping after the first model with the addition of adding objects. However, below describes our method to model the first situation as described above, using numerical methods.

The approach is to first give a problem definition, followed by a discretization. Next the spatial finite-difference is done, followed by the finite-difference in time-domain.
This model is based on the material of the course $TW3730TU$, academic year 2019-2020, which is part of the minor computational science and engineering at Delft university of technology.

B.1.1 Problem definition

The radiation propagation of waves over time in a 2D space can be described by

$$\frac{1}{c^2}\frac{\partial^2 u}{\partial t^2} = \frac{\partial^2 u}{\partial x^2} + \frac{\partial^2 u}{\partial y^2} + f = \Delta u + f \tag{19}$$

With u a physical quantity such as pressure, electric field or magnetic field. c is the propagating speed of the wave and f is some source function. We restrict ourselves to a 2D slice of the car with fixed height, width X and length Y

$$(x, y) \in (0, X) \times (0, Y) \tag{20}$$

With the domain denoted as Ω and the boundary denoted as Γ. Zero initial conditions are used to see how a wave starts propagating into space

$$\begin{aligned} u(x, y, 0) &= 0, \quad (x, y) \in \Omega \\ \left.\frac{\partial u}{\partial t}\right|_{t=0} &= 0, \quad (x, y) \in \Gamma \end{aligned} \tag{21}$$

The first model uses the most easy boundary condition, which is the following Dirichlet boundary conditions

$$u(x, y, t) = 0, \quad (x, y) \in \Gamma \tag{22}$$

B.1.2 Discretization

A double uniform grid is chosen with step size h. This gives an internal grid of $(\frac{X}{h}-1)\times(\frac{Y}{h}-1)$ grid points. The notation (x_i, y_j) is used to denote the coordinates (ih, jh).

The next step is to specify Δt. In order for the numerical solution to converge, Δt should satisfy the Courant-Friedrichs-Lewy (CFL) condition [52]

$$\frac{c\Delta t}{\sqrt{2}h} \leq 1 \tag{23}$$

B.1.3 Finite-difference in space

This section will show how Δu can be numerically approximated using the finite-difference method.
The 2D Laplacian is first decomposed into x and y

$$\Delta u = \frac{d^2u}{dx^2} + \frac{d^2u}{dy^2} \tag{24}$$

The derivation below is only done for x to avoid duplication. The variables x and y use the same step size and therefore have the same derivation.
The second partial derivative of u with respect to x at (x_i, y_j) can be described using the second-order central finite-difference as

$$\frac{d^2u_{i,j}}{dx^2} = \frac{\frac{u_{i+1,j}-u_{i,j}}{h} - \frac{u_{i,j}-u_{i-1,j}}{h}}{h} = \frac{u_{i-1,j} - 2u_{i,j} + u_{i+1,j}}{h^2} \tag{25}$$

$u_{i-1,j}$ and $u_{i+1,j}$ can both be approximated using a Taylor expansion around the known grid point $u_{i,j}$

$$\begin{aligned} u_{i-1,j} &= u_{i,j} - hu'_{i,j} + \frac{(h)^2}{2}u''_{i,j} - \frac{(h)^3}{6}u'''_{i,j} + \mathcal{O}(h)^4 \\ u_{i+1,j} &= u_{i,j} + hu'_{i,j} + \frac{(h)^2}{2}u''_{i,j} + \frac{(h)^3}{6}u'''_{i,j} + \mathcal{O}(h)^4 \end{aligned} \tag{26}$$

Combining and rewriting Equations 25 and 26 gives

$$u''_{i,j} = \frac{u_{i-1,j} - 2u_{i,j} + u_{i+1,j}}{h^2} + \mathcal{O}(h)^2 \tag{27}$$

Which is numerically approximated as

$$L_{x,i,j} = \frac{u_{i-1,j} - 2u_{i,j} + u_{i+1,j}}{(h)^2} \tag{28}$$

for all internal grid points. The structure of the $\mathbf{L}$ matrix, which is the summation of $L_x + L_y$, with dimensions $(\frac{X}{h} - 1)(\frac{Y}{h} - 1) \times (\frac{X}{h} - 1)(\frac{Y}{h} - 1)$, can be seen in figure 16, where a grid of 7×7 is used to clearly illustrate the pattern of nonzero elements. The main diagonal corresponds to the $u_{i,j}$ in Equation 28. The diagonals directly above and below the main diagonal correspond to the left and right neighbour. The two most outer diagonals are the lower and upper neighbours. This pattern is shown to emphasize the fact that this can be coded as a sparse matrix to reduce memory usage and execution time.

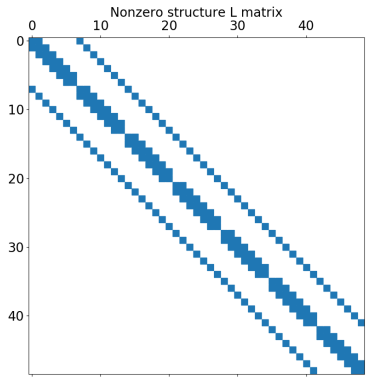

Figure 16: Nonzero pattern of L

B.1.4 Finite-difference in time

To denote $\mathbf{u}$ at time $t = i\Delta t$, the notation $\mathbf{u}^i$ is used.
The second partial derivative of u with respect to t can be approximated with the same formula as Equation 28

$$\frac{1}{c^2}\frac{\mathbf{u}^{i-1} - 2\mathbf{u}^i + \mathbf{u}^{i+1}}{\Delta t^2} = \mathbf{L}\mathbf{u}^i + \mathbf{f}^i \tag{29}$$

Which can be solved for $\mathbf{u}^{i+1}$

$$\mathbf{u}^{i+1} = (c\Delta t)^2(\mathbf{L}\mathbf{u}^i + \mathbf{f}^i) + 2\mathbf{u}^i - \mathbf{u}^{i-1} \tag{30}$$

B.1.5 Pseudo code

This section will give a short pseudo code and several plots. A Python code is used to implement the numerical scheme. The structure is to have one for-loop wherein one corresponds to a time step of Δt. $\mathbf{u}$ is updated in every iteration. The algorithm is expressed in the pseudocode given below with the final time at $t = T\Delta t$.

Algorithm 1 2D wave equation FDTD

1: **for** $i = 1, 2, \ldots, T-1, T$ **do**
2: $\quad \mathbf{f} = \mathbf{f}^i$
3: $\quad \mathbf{Lu} = \mathbf{Lu}^i$
4: $\quad \mathbf{u}^{i+1} = 2\mathbf{u}^i$ - $\mathbf{u}^{i-1}$ + $(c\Delta t)^2\mathbf{Lu}$ + $(c\Delta t)^2\mathbf{f}$
5: $\quad \mathbf{u}^{i-1} = \mathbf{u}^i$
6: $\quad \mathbf{u}^i = \mathbf{u}^{i+1}$
7: **end for**

B.1.6 Plots

An isotropic source modeled as a point-source at (X_0, Y_0) can be modeled as $f(t)e^{\alpha(x-X_0)^2+\alpha(y-Y_0)^2}$ with α a large negative constant. An example of the wave propagation pattern for such a

source in an empty Ω is given in Figure 17, where f(t) is defined as $-cos(\Omega t)$ placed at the center of Ω. To improve the resolution of the plots, a larger grid is used than a typical car. It is clearly visible that the waves propagates in all directions and reflects at the boundary of Ω.

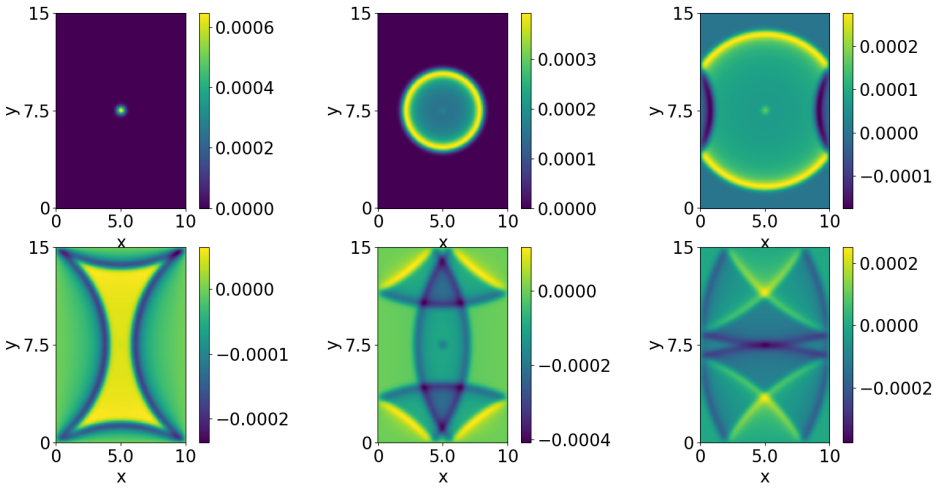

Figure 17: Wave propagation of a CW point-source

A pulsed source function is modeled as described in section 4.2.2 and can be seen in Figure 18. The upper-left, upper-right and center-bottom are time-snaps right after a new pulse was emitted.

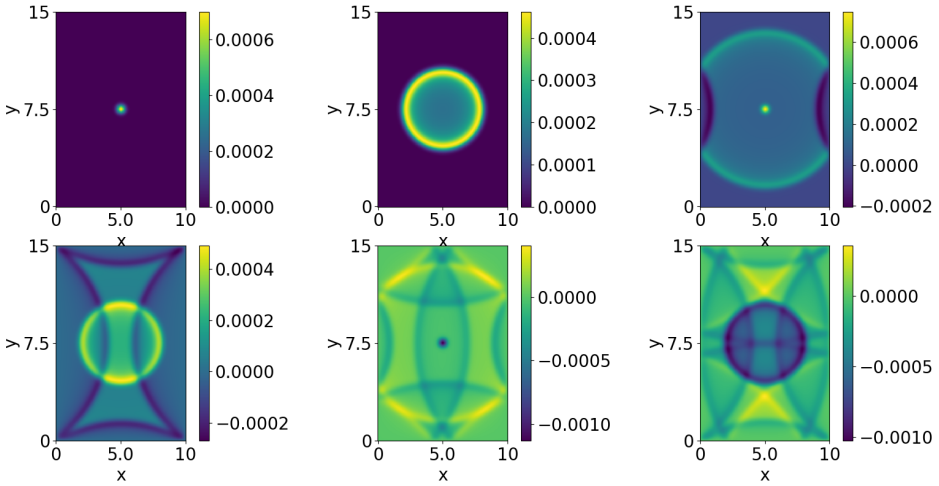

Figure 18: Wave propagation of a pulsed point-source

B.1.7 Difficulties

Difficulties occurred when the spatial step size h was decreased. This decrease was necessary for decreasing wavelength. The size of the Laplacian matrix L is $\mathcal{O}(\frac{1}{h})^4$, which gives already memory issues when h is set to 1mm. Because respiration displacement is in the order of mm, the resolution of the simulation would be insufficient.
The simulation was considered as a bonus, which why it was chosen to stop spending time in the simulation at that point.

A few likely problems that might have occurred later in the simulation when there was more time. A few of these are described below.
A problem that would have happened later was the velocity of the baby's chest movement due to respiration. This velocity is much lower than the speed of light. All displacements in the grid are discretized in the order of h. This would mean that h should be made very small, such that the velocity of the chest movement and the velocity of the EM wave are in the right scale with respect to each other. However the size of the Laplacian matrix is $\mathcal{O}(h)^4$, which would throw a memory error for small h. When neglecting to downsize the h, the displacement of the baby's chest will be either constantly rounded down or unrealistically large. This will make the use of the Doppler shift very difficult.

When more time was available for the simulation, research would have been done on implementing an absorbing boundary condition. This boundary condition would allow partial transmission and reflection instead of total reflection.

C Appendix C

C.1 Infrared respiration rate

Figure 19 describes the steps of how the respiration rate would be extracted from the thermal video acquired in Section 5.3. Four time signals of the temperature in the nasal and oral area are extracted from the video. A selection of the best signal is done based on the signal quality index (SQI) of the signals, calculated by the ratio between power spectral density (PSD), autocorrelation (ACR) and cross-power spectral density (CPSD). The following two rules applies:

1. Rule 1 (nasal SQI): If the ratio of RR_{PSD} nose to RR_{ACR} nose and that of RR_{PSD} nose to RR_{CSPD} nose obtained by the nasal area lie between 0.85 and 1.15, the *nasal temperature* is selected as the respiration signal.

2. Rule 2 (oral SQI): If the ratio of RR_{PSD} mouth to RR_{ACR} mouth and that of RR_{PSD} mouth to RR_{CSPD} mouth obtained by the oral area lie between 0.85 and 1.15, the *oral temperature* change is selected as the respiration signal.

Eventually, the respiration rate is obtained by the multiple signal classification (MUSIC) algorithm.

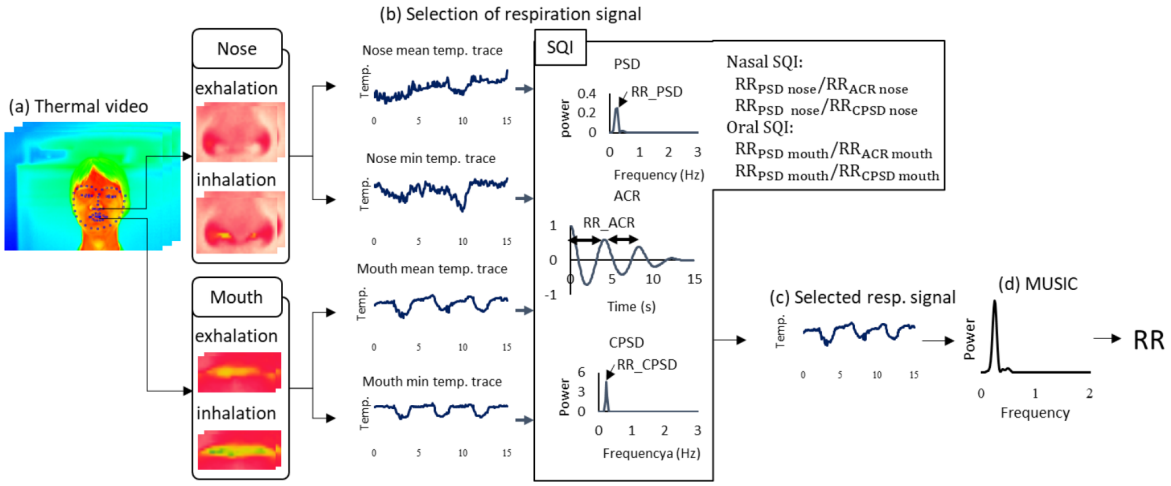

Figure 19: Block diagram of signal processing for respiration detection and estimation. (a) Thermal video frame with facial landmark detected by the fusion sensor system described in Section 5.3. (b) Time-series data extracted from nasal and oral areas. (c) Respiration signal chosen from the four signals in (b) based on SQI. (d) Power spectrum obtained by MUSIC algorithm [38]

C.2 Optical camera heartbeat

The camera-based heartbeat detection is as follows. First, facial video is collected over a certain period. Then the facial images are separated into the three RGB channels, as shown in Figure 20, and the resulting two-dimensional images are transformed into one-dimensional time-series signals. Each channel signal is normalized, detrended and processed using the independent component analysis (ICA) to remove noise components. At the output of the ICA, we have three independent signals in a random order.

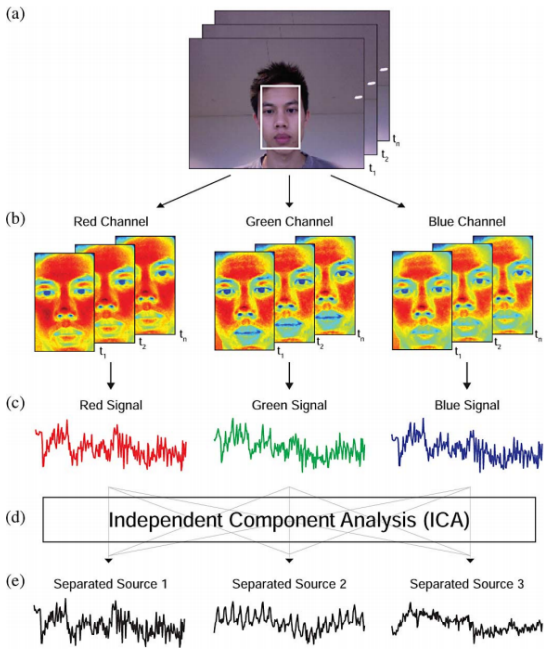

Figure 20: Recovery of the BVP waveform. (a) Face within the first video frame is automatically detected to locate the ROI. (b) ROI is decomposed into red, green, and blue channels for each frame and spatially averaged to form (c) the raw signals. After the raw signals are detrended and normalized, ICA is applied to separate three independent sources. In this example, the BVP is visible in the second source signal [41].

Afterwards, as shown in Figure 21, the signals are filtered via bandpass filtering, in this case a tapered window, and estimated with the Fast Fourier Transformation (FFT). The signals are then reconstructed, for instance with a signal reconstruction method based on SoftSig [53], so that the heart rate can be clearly extracted from its spectrum.

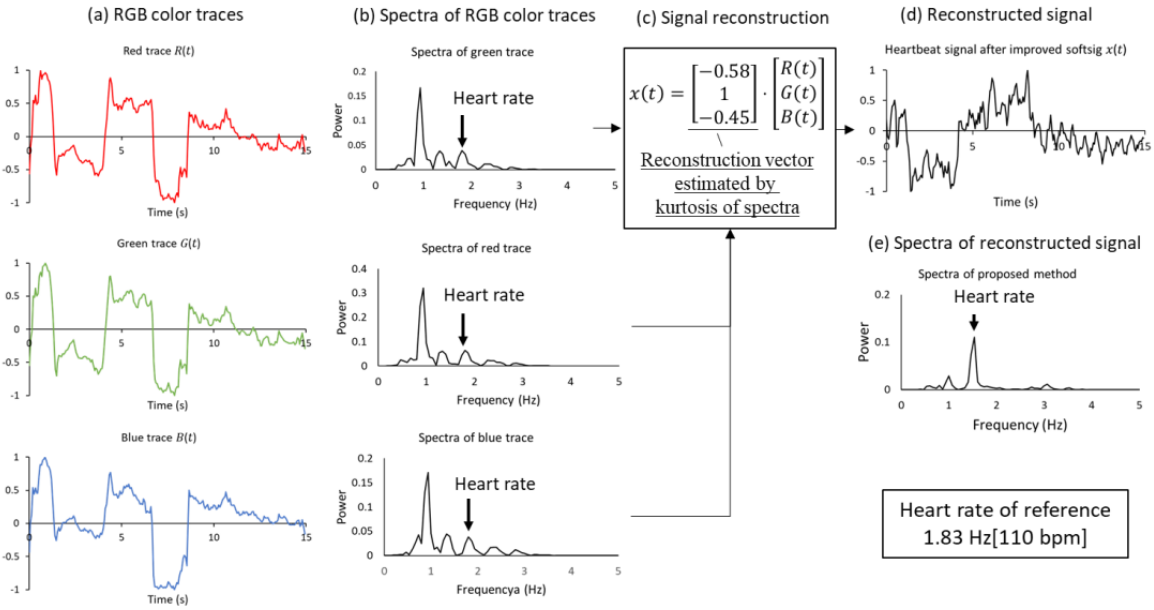

Figure 21: (a) RGB color traces obtained by RGB video. (b) Spectra estimated by Fast Fourier Transform (FFT). (c) Signal reconstruction determined through kurtosis of the spectra. (d), (e) Reconstructed signal and its spectra. [38]